

Contract Program or Project Title: Heavy-Section Steel Irradiation Program,
Metals and Ceramics Division

Subject of this Document: Comparison of Effects of Thermal Aging,
Irradiation, and Thermal Annealing on the
Propensity for Temper Embrittlement on
an RPV Submerged-Arc Weld HAZ

Type of Document: ORNL Letter Report

Authors: R. K. Nanstad, D. E. McCabe, and
M. A. Sokolov - Oak Ridge National
Laboratory, Oak Ridge, Tennessee

C. A. English, and S. R. Ortner -
AEA-Technology, Harwell,
United Kingdom

Date of Document: December 2001

**Responsible NRC Individual and
NRC Office or Division:** C. J. Fairbanks, 301-415-6719
Division of Engineering Technology
Office of Nuclear Regulatory Research

Prepared for the
U.S. Nuclear Regulatory Commission
Office of Nuclear Regulatory Research
Under Interagency Agreement DOE 1886-N695-3W

NRC JCN W6953

Prepared by the
OAK RIDGE NATIONAL LABORATORY
Oak Ridge, TN 37831-6151
Managed by
UT-Battelle, LLC
for the
U.S. DEPARTMENT OF ENERGY
Under Contract No. DE-AC05-00OR22725

Comparison of Effects of Thermal Aging, Irradiation, and Thermal Annealing on the
Propensity for Temper Embrittlement on an RPV Submerged-Arc Weld HAZ

R. K. Nanstad, D. E. McCabe, and M. A. Sokolov
Oak Ridge National Laboratory, Oak Ridge, Tennessee

C. A. English, and S. R. Ortner -
AEA-Technology, Harwell, United Kingdom

Date Published —December 2001

Prepared for the
U.S. Nuclear Regulatory Commission
Office of Nuclear Regulatory Research
Under Interagency Agreement DOE 1886-N695-3W

NRC JCN W6953

Prepared by
OAK RIDGE NATIONAL LABORATORY
Oak Ridge, TN 37831-6151
managed by
UT-Battelle, LLC
for the
U.S. Department of Energy
Under Contract No. DE-AC05-00OR22725

CONTENTS

| | |
|--|-----|
| TABLES | v |
| FIGURES | vii |
| ACRONYMS AND ABBREVIATIONS | ix |
| ABSTRACT | 1 |
| INTRODUCTION | 2 |
| AEA-TECHNOLOGY EVALUATION OF RPV STEELS | 5 |
| ORNL TEMPER EMBRITTLEMENT STUDIES | 5 |
| Results of Temper Embrittlement Studies | 9 |
| Measurement of Element Diffusion to Grain Boundaries | 15 |
| Effects of Irradiation and Thermal Annealing | 18 |
| DISCUSSION | 19 |
| SUMMARY OF OBSERVATIONS AND CONCLUSIONS | 26 |
| ACKNOWLEDGMENTS | 27 |
| REFERENCES | 28 |

TABLES

| | | |
|-----------|--|----|
| Table 1. | Summary of AEA-Technology Temper Embrittlement Results | 5 |
| Table 2. | Commercial Materials Used for ORNL Temper Embrittlement Studies | 7 |
| Table 3. | Chemical Composition and Tensile Properties of Materials for ORNL Temper Embrittlement Studies | 8 |
| Table 4. | As-received tensile properties | 8 |
| Table 5. | Grain Sizes of the Commercially Made Materials in the As-Received Condition | 9 |
| Table 6. | Effects of Thermal Aging on Five RPV Steels Given the AEA Heat Treatment | 11 |
| Table 7. | Charpy Impact Transition Temperatures for ORNL Materials Austenitized by Gleeble, PWHT, and Thermal Aging | 14 |
| Table 8. | Largest Coarse Grain Sizes Found in HAZs of Six Commercially Fabricated RPV Welds | 15 |
| Table 9. | AEA-Technology Measurements of Grain Boundary Phosphorus Coverage | 15 |
| Table 10. | Results of Auger Analysis on A533 Steel in the Gleeble/PWHT Condition Aged at 450°C (842°F) for 2000 h | 18 |
| Table 11. | Summary of Irradiation, Annealing, and Thermal Aging Effects on Simulated HAZ in A302B (Modified) Steel | 19 |

FIGURES

| | | |
|------------|---|----|
| Figure 1. | Schematic representation of microstructures local to the HAZ of multipass welds | 3 |
| Figure 2. | Cumulative number of chemical samplings made on RPV base metals versus the phosphorus content | 6 |
| Figure 3. | Example of the typical microstructure after the AEA-Technology austenitize, quench, and postweld heat treatment, A533 grade B steel, nital etch, 100× | 10 |
| Figure 4. | Gleeble-generated weld thermal cycle to develop ASTM 4.5 grain size | 13 |
| Figure 5. | Photomicrograph of the microstructure of the high-phosphorus modified A302 grade B steel after Gleeble austenitize and postweld heat treatment, nital etch, 100× | 13 |
| Figure 6. | Charpy impact mid-transition temperatures after aging for 168 h at 399, 450, and 482 °C (750, 842, and 900 °F) and 2000 h at 450 °C (MA302B) | 16 |
| Figure 7. | Auger analysis of phosphorus concentration in A533 grade B class 1 following Gleeble austenization and thermal aging at 450 °C (842 °F) for 2000 h | 17 |
| Figure 8. | Scanning electron fractograph of as-received modified A302B steel Charpy impact specimen following irradiation at 288 °C (550 °F) to 1×10^{19} n/cm ² | 20 |
| Figure 9. | Scanning electron fractograph of Gleeble austenitized/PWHT modified A302B steel Charpy impact specimen following irradiation at 288 °C (550 °F) to 1×10^{19} n/cm ² | 21 |
| Figure 10. | Scanning electron fractograph of Gleeble austenitized/PWHT modified A302B steel Charpy impact specimen following irradiation at 288 °C (550 °F) to 1×10^{19} n/cm ² and thermal annealing at 460 °C (860 °F) for 168 h | 22 |
| Figure 11. | Scanning electron fractograph of Gleeble austenitized/PWHT modified A302B steel Charpy impact specimen following irradiation at 288 °C (550 °F) to 1×10^{19} n/cm ² and thermal annealing at 460 °C (860 °F) for 168 h | 23 |
| Figure 12. | Scanning electron fractographs of Gleeble austenitized/PWHT modified A302B steel Charpy impact specimen following irradiation at 288 °C (550 °F) to 1×10^{19} n/cm ² and thermal annealing at 460 °C (860 °F) for 168 h showing (a) region near crack front and (b) region near one side of the specimen showing shear lip area | 24 |

ACRONYMS AND ABBREVIATIONS

| | |
|--------|---|
| CE | carbon equivalent |
| CGHAZ | coarse-grain heat-affected zone |
| CVN | Charpy V-notch |
| EDX | energy-dispersive X-ray |
| FGHAZ | fine-grain heat-affected zone |
| GB | grain boundary |
| HAZ | heat-affected zone |
| HSSI | Heavy Section Steel Irradiation (Program) |
| IAR | Irradiation, Annealing, and Reirradiation |
| LBZ | local brittle zone |
| LSE | lower-shelf energy |
| NRC | U.S. Nuclear Regulatory Commission |
| ORNL | Oak Ridge National Laboratory |
| PWHT | postweld heat treatment |
| RPV | reactor pressure vessel |
| SAW | submerged-arc weld |
| SMAW | shielded metal-arc weld |
| SNUPPS | Standardized Nuclear Power Plant System |
| SP | sputtering |
| STEM | scanning transmission electron microscope |
| TG | transgranular cleavage |
| USE | upper-shelf energy |

COMPARISON OF EFFECTS OF THERMAL AGING, IRRADIATION, AND THERMAL ANNEALING ON THE PROPENSITY FOR TEMPER EMBRITTELEMENT ON AN RPV SUBMERGED-ARC WELD HAZ

**R. K. Nanstad, D. E. McCabe, and M. A. Sokolov
Oak Ridge National Laboratory**

**C. A. English and S. R. Ortner
AEA-Technology, Harwell, U.K.**

ABSTRACT

The Heavy-Section Steel Irradiation Program at Oak Ridge National Laboratory includes a task to investigate the propensity for temper embrittlement in coarse grain regions of heat-affected zones in prototypic reactor pressure vessel (RPV) steel weldments as a consequence of irradiation and thermal annealing. For the present studies, five prototypic RPV steels with specifications of A302 grade B, A302 grade B (modified) (two heats), A533 grade B class 1, and A508 class 2 were given two different austenitization treatments and various thermal-aging treatments. The thermal-aging treatments were conducted at 399, 425, 454 and 490°C (750, 797, 850, and 915°F) for times of 168 and 2000 h. Charpy V-notch impact toughness vs temperature curves were developed for each condition with ductile-brittle transition temperatures used as the basis for comparing the effects of the various heat treatments. Very-high-temperature austenitization heat treatment produced extremely large grains that exhibited a very high propensity for temper embrittlement following thermal aging. Intergranular fracture was the predominant mode of failure in many of the materials, and Auger analysis confirmed significant segregation of phosphorus at the grain boundaries. Lower-temperature austenitization treatment performed in a super Gleeble to simulate prototypic coarse grain microstructures in submerged-arc weldments produced the expected grain size with varying propensities for temper embrittlement, dependent on the material as well as on the thermal-aging temperature and time. Although the lower-temperature treatment resulted in a decreased propensity for temper embrittlement, the results provided motivation for the investigation of the potential for phosphorus segregation as a consequence of neutron irradiation and postirradiation thermal annealing at 454°C (849°F). The McClean model of phosphorus segregation reasonably predicted the measured results. One of the A 302 grade B (modified) steels was given the Gleeble treatment, was irradiated at 288°C (550°F) to about 0.8×10^{19} n/cm² (>1 MeV) and was given a thermal annealing treatment at 454°C for 168 h. Charpy impact testing was conducted on the material in both the irradiated and irradiated/annealed conditions as well as in the as-received condition. The results show that the simulated heat-affected-zone material exhibited significant intergranular fracture in the postirradiation annealed condition, although it exhibited a relatively small Charpy impact 41-J temperature shift.

INTRODUCTION

In 1989, Combustion Engineering proposed to the U.S. Nuclear Regulatory Commission (NRC) that consideration be given to replacing the fracture-toughness-based dynamic K_{IR} curve with the quasi-static K_{Ic} curve for setting allowable temperature/pressure limits during normal upset conditions¹. The idea was accepted for consideration pending the development of clear evidence that there can be no unanticipated trigger sources that would introduce running cleavage cracks. Such sources could be either crack pop-ins or possibly local brittle zones (LBZs) that reside along the fusion line of multipass weldments. The existence of LBZs was suggested as one of the possibilities for reactor pressure vessel (RPV) weldments. The NRC asked the Heavy-Section Steel Irradiation (HSSI) Program at Oak Ridge National Laboratory (ORNL) to review the available LBZ information, to determine its applicability to nuclear vessel fabrication and service conditions, and to conduct experiments in support of the evaluations. A detailed discussion of the LBZ evaluation was presented by McCabe [1], from which the unirradiated temper embrittlement results reported here were taken. Part of the overall study was a consideration of the effects of irradiation and thermal annealing on the coarse grain region of the heat-affected zone (HAZ) in a submerged-arc weldment. Research projects designed to evaluate LBZ damage mechanisms generally use electric resistance heating of specimen blanks to simulate material that has been through a weld pass cycle [2,3,4]. Brittle-zone microstructures are created in sufficient bulk to develop reliable Charpy transition curves that represent the various microstructures identified within the LBZ region.

The thermal history and consequent morphology of HAZ welds are extremely complex. Each weld pass produces a four-zone microstructural gradient (see Fig. 1). The coarse grain HAZ (CGHAZ) (Fig. 1D), immediately adjacent to the fusion line, consists of enlarged prior austenite grains from the subsequent weld passes that grow rapidly due to being at a temperature close to the melting point. Upon cooling, the prior austenite can transform to martensite or a lower bainite-martensite mix, depending on the carbon equivalent (CE) of the base metal. At slow cooling rates, low-CE steels will transform to a lower-toughness microstructure (pearlite and/or upper bainite). With low CE, the cooling rate must be quite rapid for martensite and lower bainite to form. Lower bainite and/or martensitic steel is more brittle as cooled, but these microstructures are converted to high-toughness steel after postweld heat treatment (PWHT). The second zone from the fusion line, fine-grain HAZ (FGHAZ) (Fig. 1C), is fine-grain prior austenite resulting from slower austenitic grain growth at lower temperatures. The third zone, intercritical coarse grain HAZ (ICCGHAZ) (Fig. 1B), is material heated into the A_{c3} and A_{c1} (intercritical) transformation zone. A mixture of ferrite and austenite precipitates along prior austenite grain boundaries, which embrittles the material in this local region upon

¹R. K. Nanstad, notes from meeting with the U.S. Nuclear Regulatory Commission, January 9, 1990.

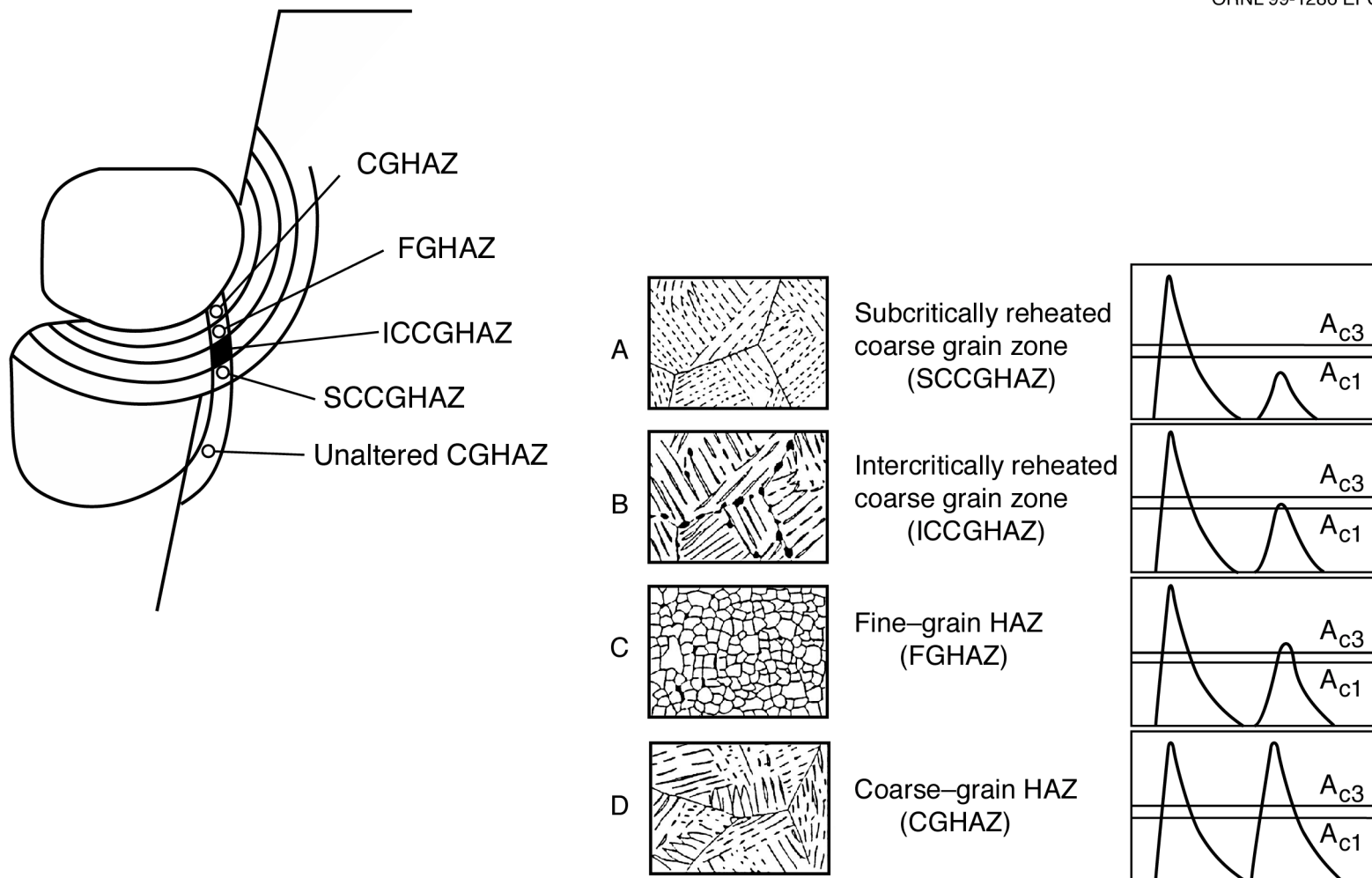


Figure 1. Schematic representation of microstructures local to the HAZ of multipass welds.

cooling to room temperature [2,3]. These small volumes of ICCG HAZ material have been identified as the LBZ trigger-point locations. It is understood that LBZ material is created by the reheating of coarse grain prior austenite from the subsequent weld passes that are adjacent to the fusion line. It therefore follows that there can be an appreciable amount of coarse grain prior austenite along a fusion line that is not brittle crack-initiation material. The fourth zone is the subcritical reheated coarse grain zone (SCCGHAZ) (Fig. 1A), which undergoes very little change in properties. An interesting outcome of the fundamental studies on microalloyed steels has been a demonstration that ICCG HAZ microstructures can cause a transition temperature increase of about 15 to 20°C over that of unsensitized material [3]. When these materials are postweld heat treated at 450°C (842°F), the fracture toughness of ICCG HAZ material is restored and, in some cases, slightly improved over that of the unsensitized condition.

RPV weldments are principally multipass submerged-arc welds (SAWs) with high heat input that can promote the development of coarse prior austenite grains. CE is important from the standpoint of the transformation products formed on cooldown. Several important alloying elements contribute to CE, as indicated from the following equation:

$$CE = \frac{Mn}{6} + \frac{Cu + Ni}{15} + \frac{Mo + V + Cr}{5}. \quad (1)$$

The CE controls austenite stability and hence promotes transformation to low-temperature transformation constituents such as lower bainite and martensite. The typical CE in low-carbon microalloyed steel is about 0.37, whereas the typical RPV steel has a CE of about 0.62. Increased CE generally decreases weldability; the steel has an increased propensity for cracking because the transformation products tend to become embrittled as they cool. However, postweld tempering converts the steel to one with excellent fracture toughness properties.

If postirradiation thermal annealing is to be used, the service temperature cycle could include a 168-h excursion to 482°C (900°F) for a one-time cycle. Thus, the concern regarding coarse grain regions in RPV welds arises from the potential for metallurgical degradation by temper embrittlement. Only the HAZ is at issue because RPV steel plates and forgings usually have fine prior austenite grains and, as a consequence, the base materials are not considered to be vulnerable to temper embrittlement.

AEA-TECHNOLOGY EVALUATION OF RPV STEELS

The embrittlement susceptibility of grain-coarsened RPV steels was clearly demonstrated in work at AEA-Technology, Harwell, United Kingdom [5]. Eleven laboratory heats of steel with typical RPV chemical composition (i.e., similar to A533 grade B class 1) were made, and three of these with varied copper and phosphorus contents were selected for temper embrittlement studies. The sensitivity to embrittlement was enhanced by heat treating to obtain very large prior austenite grain size [about 0 to 1 per ASTM Standard Test Methods for Determining Average Grain Size (E 112)]. The austenitization temperature was 1200°C (2200°F) with a 30-min soak followed by an oil quench. All were given PWHT at 615°C (1140°F) with a 24-h soak and again followed by an oil quench. The AEA-Technology temper embrittlement aging was 450°C (842°F) for 2000 h for the fully aged condition and 475° (890°F) to simulate an end-of-life recovery anneal cycle. One other exposure was irradiation to 12.2 mdpa at 288°C (550°F). Table 1 provides a summary of AEA's findings. It is important to keep in mind that the ΔT_0 values are extremely dependent on grain size, and with grain sizes of ASTM 0 to 1, the above results may not truly represent the coarse grain microstructure in RPV weld HAZs.

Table 1. Summary of AEA-Technology Temper Embrittlement Results

| Chemistry variable (wt %) | | Aging (h/°C) | Charpy impact T_0 (°C) | | Charpy impact ΔT_0 (°C) |
|------------------------------------|-------|-----------------|--------------------------------|------|--|
| Cu | P | | Initial | Aged | |
| 0.01 | 0.007 | 2000/450 | -86 | 32 | 118 |
| 0.01 | 0.017 | 2000/450 | -55 | 119 | 174 |
| 0.16 | 0.017 | 2000/450 | -95 | 114 | 209 |
| 0.16 | 0.017 | <i>a</i> | -95 | -26 | 69 |
| ^a Irradiated 12.5 mdpa. | | | | | |

ORNL TEMPER EMBRITTLEMENT STUDIES

Five commercially produced RPV steels were selected for the present program; their reported chemical elements are shown in Table 2. These as-reported analyses served as the basis of selection for the materials to be evaluated. An objective was to include at least one material with the phosphorus level considered to be as high as that in the AEA-Technology experiment (Table 1). High copper, by the AEA-Technology definition, was almost automatic in the commercial steels that were available. The high phosphorus,

on the other hand, was not as easily obtained because that level of phosphorus is quite high for U.S. RPV base metals, as shown in Fig. 2 [6].

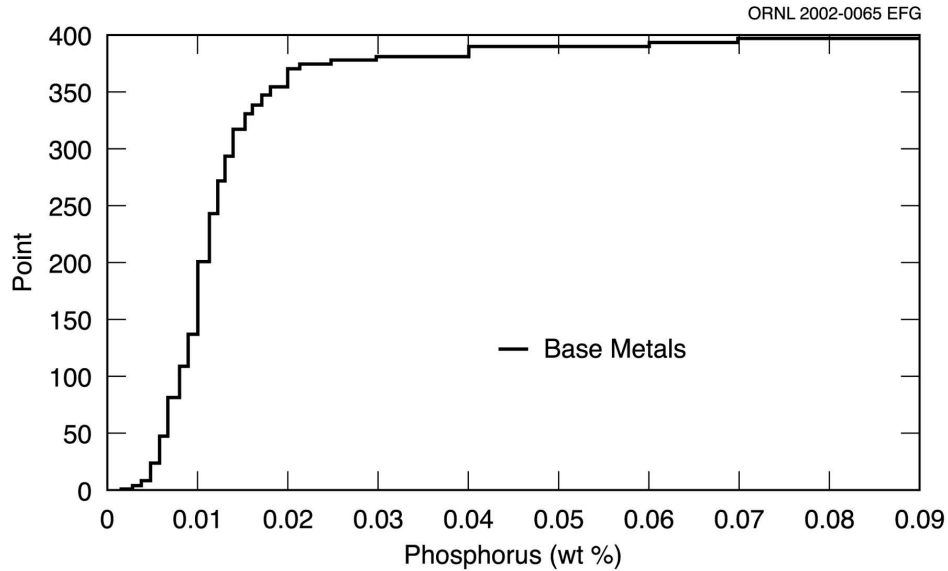


Figure 2. Cumulative number of chemical samplings made on RPV base metals versus the phosphorus content.

Confirmatory chemical analyses and tensile properties were obtained during the course of the present investigation, and these properties are reported along with the as-received values in Tables 3 and 4. The initially reported chemical compositions were not entirely reliable, as can be seen. One material, A 302 grade B, received in the as-normalized condition, was not available in the desired heat-treated condition. Consequently, the normalized microstructure was converted into a quenched-and-tempered product using a double austenitize, quench, and temper treatment [1]. This treatment simulated the heat treatment reported on the low-phosphorus modified A 302 grade B steel listed in Table 2. This particular modified A 302 grade B (Z7) came from a commercial reactor nozzle cutout. The end result was suitable from a mechanical-properties standpoint, but it was later determined that the quenched-and-tempered microstructure had prior austenite grain size of ASTM 5, which was large in comparison with those of the other commercially made steels (Table 5).

Table 2. Commercial Materials Used for ORNL Temper Embrittlement Studies

| Material | Source code | Content ^a (wt %) | | | |
|------------------------|---------------|--------------------------------|------|-------|------|
| | | P | Ni | S | Cu |
| A 302 grade B | Maine Yankee | 0.015 | 0.2 | 0.017 | 0.14 |
| A 508 class 2 | Midland | 0.010 | 0.76 | 0.015 | 0.02 |
| Modified A 302 grade B | GE (Z5) | 0.016 | 0.62 | 0.015 | 0.17 |
| Modified A 302 grade B | GE (Z7) | 0.007 | 0.53 | 0.014 | 0.16 |
| A 533 grade B | HSST Plate 01 | 0.018 | 0.75 | 0.013 | 0.18 |

^aComposition from material supplier; see Table 3 for detailed analysis.

The general plan to evaluate temper embrittlement in the five RPV steels was structured to be in three phases, starting with the AEA-Technology heat-treatment schedule discussed earlier, except that in this case commercially produced RPV steels were used. The three phases are defined as follows.

Phase I - Simulate the AEA-Technology heat treatment. Austenitize at 1200°C (2200°F) for 30 min, oil quench, postweld heat treat at 615°C (1140°F) for 24 h, oil quench, and age by two different aging treatments:

1. Age for 2000 h at 450°C (842°F).
2. Age for 168 h at 490°C (914°F).

Phase II - Use electric resistance heating (Gleeble) to simulate a typical SAW cycle to develop the coarse grain microstructure. Austenitize at 1260°C (2300°F) for 10 s, postweld heat treat at 615°C (1140°F) for 24 h, oil quench, and age by two different aging treatments:

1. Age for 2000 h at 450°C (842°F).
2. Age 168 h at 450°C (842°F).

Note: The rapid cool following PWHT should maximize the temper embrittlement susceptibility.

Phase III - Perform the same heat-treatment schedule as in Phase II. Follow heat treatment with two different aging cycles, an irradiation cycle, and an irradiation/thermal annealing cycle:

1. Age for 168 h at 482°C (900°F).
2. Age for 168 h at 399°C (750°F).
3. Irradiate to 1×10^{19} n/cm² [>1 MeV at 288°C (550°F)].
4. Irradiate to 1×10^{19} n/cm² [>1 MeV at 288°C (550°F)], then anneal for 168 h at 450°C (842°F).

Table 3. Chemical Composition and Tensile Properties of Materials for ORNL Temper Embrittlement Studies

| Material | Condition ^a | Composition (wt %) | | | | | | | | | | | | |
|--------------|------------------------|--------------------|------|-------|-------|------|------|------|------|-------|-------|------|-------|-------|
| | | C | Mn | P | S | Si | Ni | Cr | Mo | V | Nb | Cu | As | Sn |
| A302B | AR | 0.21 | 1.20 | 0.015 | 0.015 | 0.28 | 0.19 | 0.24 | 0.60 | 0.004 | 0.006 | 0.13 | 0.015 | 0.012 |
| | AEA | 0.21 | 1.15 | 0.014 | 0.016 | 0.31 | 0.21 | 0.22 | 0.57 | 0.005 | 0.005 | 0.14 | 0.018 | 0.011 |
| | AS | 0.22 | 1.12 | 0.014 | 0.015 | 0.31 | 0.18 | 0.21 | 0.56 | 0.005 | 0.003 | 0.15 | 0.17 | 0.010 |
| A508 class 2 | AR | 0.20 | 0.63 | 0.009 | 0.013 | 0.19 | 0.75 | 0.37 | 0.60 | <0.01 | — | 0.02 | <0.01 | <0.01 |
| | AEA | 0.22 | 1.04 | 0.013 | 0.010 | 0.28 | 0.73 | 0.21 | 0.57 | 0.002 | 0.004 | 0.05 | 0.015 | 0.006 |
| Mod A302B | AR | 0.17 | 1.27 | 0.014 | 0.016 | 0.17 | 0.61 | 0.10 | 0.50 | 0.002 | 0.004 | 0.16 | 0.013 | 0.017 |
| | AEA | 0.20 | 1.12 | 0.015 | 0.018 | 0.19 | 0.61 | 0.09 | 0.47 | 0.003 | 0.005 | 0.18 | 0.018 | 0.016 |
| Mod A302B | AR | 0.19 | 1.10 | 0.016 | 0.017 | 0.19 | 0.54 | 0.09 | 0.46 | 0.003 | 0.003 | 0.19 | 0.017 | 0.015 |
| | AEA | 0.26 | 1.47 | 0.08 | 0.014 | 0.15 | 0.53 | 0.09 | 0.52 | 0.002 | 0.003 | 0.16 | 0.014 | 0.018 |
| A533B | AR | 0.24 | 1.34 | 0.016 | 0.013 | 0.23 | 0.80 | — | 0.53 | — | — | — | — | — |
| | AEA | 0.23 | 1.15 | 0.010 | 0.012 | 0.28 | 0.74 | 0.10 | 0.55 | 0.003 | 0.004 | 0.12 | 0.013 | 0.010 |
| | AS | 0.22 | 1.49 | 0.010 | 0.012 | 0.27 | 0.65 | 0.10 | 0.55 | 0.003 | 0.004 | 0.20 | 0.020 | 0.015 |

^aAR = As reported; AEA = AEA + 2000 h at 450°C; AS = as-received and aged.

Table 4. As-received tensile properties

| Material | Yield strength | | Tensile strength | |
|--------------|----------------|-------|------------------|-------|
| | (MPa) | (ksi) | (MPa) | (ksi) |
| A302B | 538 | 78.1 | 689 | 100.1 |
| A508 class 2 | 394 | 57.1 | 569 | 82.6 |
| A533 grade B | 470 | 68.2 | 620 | 89.9 |
| Mod A302B Z5 | 400 | 58.1 | 538 | 78.1 |
| Mod A302B Z7 | 472 | 68.5 | 632 | 91.7 |

Table 5. Grain Sizes of the Commercially Made Materials in the As-Received Condition

| Material | Size by E 112 | Average grain diameter (μm) |
|--|---------------|-----------------------------|
| A302 grade B ^a | 5 | 65 |
| A508 class 2 | 8 | 22 |
| A533 grade B | 8.5 | 19 |
| Mod A302 grade B Z5 | 10 | 11 |
| Mod A302 grade B Z7 | 9 | 16 |
| ^a Reprocessed from normalized to quenched and tempered. | | |

Additionally, baseline Charpy V-notch (CVN) data were generated to provide the unaged condition in each case to quantify transition temperature shifts and to supplement the metallurgical evaluations. In all cases, temper embrittlement was evaluated by CVN transition curve shifts.

Results of Temper Embrittlement Studies

Phase I - All of the commercially produced steels that were given the AEA-Technology heat-treatment cycle had martensite to lower bainite microstructures. Grain size by ASTM Standard E 112 was generally between 0 and 00, meaning that the typical austenite grain diameter was on the order of 360 to 500 μm. The microstructure after PWHT is shown in Fig. 3.

The CVN energy, E_j , data were least-squares fitted to the following hyperbolic tangent equation:

$$E_j = A + B \tanh [(T - T_o)/C] , \quad (2)$$

where

- A = (USE + LSE)/2,
- B = (USE - LSE)/2,
- C = width of the transition,
- T_o = mid-transition temperature,
- USE = upper-shelf energy,
- LSE = lower-shelf energy, fixed at 2.7 J.

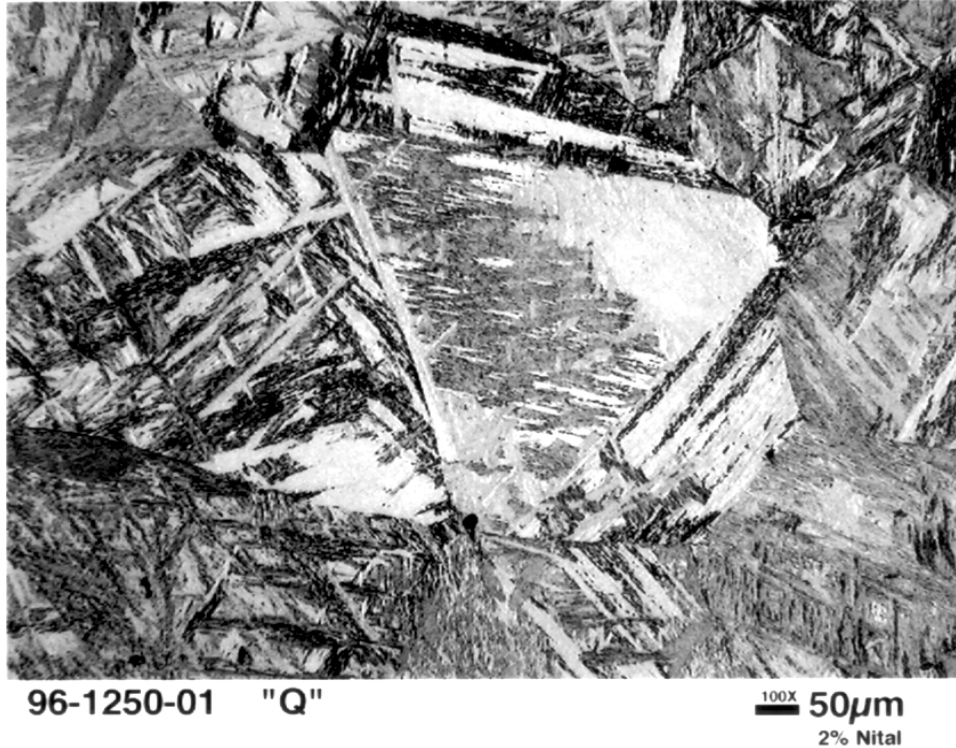


Figure 3. Example of the typical microstructure after the AEA-Technology austenitize, quench, and postweld heat treatment, A533 grade B steel, nital etch, 100×.

Parameter, T_0 was selected to be the transition curve temperature level of reference. T_0 is a point halfway between the lower-shelf and upper-shelf Charpy energy. This point was selected because it tends to be a position that is least affected by changes in curve shape. The LSE used in fitting data to Eq. (2) was held constant at 2.7 J [7,8].

Table 6 lists the CVN T_0 temperatures of the five commercial RPV steels in the as-received condition, both before and after embrittlement aging. As-received RPV steels with small grains on the order of ASTM 8 to 11 showed insignificant embrittlement. The A302 grade B exception ($\Delta T_0 = 64^\circ\text{C}$) was caused by larger grains (on the order of 5). Aging of the materials following austenitization and PWHT to simulate the AEA-Technology heat-treatment schedule showed aging-induced transition temperature shifts from 12 to 145°C, with the aging at 450°C (842°F) for 2000 h causing greater embrittlement than those at 490°C (914°F) for 168 h.

In summary, the results from the Phase I study (to simulate the AEA-Technology experiments using commercially made steels) showed that only two of the five steels exhibited temper embrittlement similar to the level of the AEA-Technology experiments. The conversion to large prior austenite grains by the AEA-Technology austenitizing

Table 6. Effects of Thermal Aging on Five RPV Steels Given the AEA Heat Treatment

| Condition ^a | Aging time (h) | Aging temperature (°C) | Charpy impact transition temperature, T ₀ (°C) | | | | |
|--|----------------|------------------------|---|-------|--------------|----------------|-------|
| | | | A302B | A533B | A508 class 2 | Modified A302B | |
| | | | | | | High P | Low P |
| As received | Initial | — | 0 | 20 | 0 | -9 | -9 |
| As received | 2000 | 450 | 64 | 38 | 10 | -4 | 10 |
| AEA austenitize ^b and PWHT ^c | Initial | — | 10 | -67 | 4 | -23 | -73 |
| AEA austenitize ^b and PWHT ^c | 2000 | 450 | 45 | 78 | 41 | 34 | 42 |
| AEA austenitize ^b and PWHT ^c | 168 | 490 | 44 | 65 | 16 | 16 | -3 |

^aAverage grain sizes range from 360 to 500 μm (ASTM 0 to 00)
^b30 min at 1200°C; oil quench.
^c24 h at 615°C; oil quench.

treatment by itself did not always cause significant change in toughness from the as-received toughness. For example, as a result of the AEA-Technology heat treatment, there were small increases in T_o for two materials, while the other three changes in T_o were negative, with two of these being substantial (compare rows 1 and 3 in Table 6). The dependence of ΔT_o on prior-austenite grain size was clearly demonstrated in four of the five materials tested and was weakly demonstrated in the fifth. However, the grain sizes that resulted from the AEA-Technology austenitizing treatment were considerably larger than those expected in actual ICCGHAZ regions, suggesting that these Phase I results do not truly represent the coarse grain situation of interest in commercial RPV welds. They do, however, demonstrate the susceptibility of these commercial steels to temper embrittlement and provide the motivation for further study with more prototypical microstructures.

Phases II and III - The electrical resistance method of heating and cooling with equipment designed specifically for simulation of weld cycles (Gleeble, Inc.) was applied to austenitize the same five materials tested in Phase I. Because the intercritical reheating cycle, identified as the source of LBZ behavior in low-carbon microalloyed steels, was determined to be of no relevance to RPV steels, only a single simulation cycle was needed in the present experiment to simply create the simulated coarse prior austenite grains in RPV HAZs. A report by Lundin and Mohammed [9] was used to decide upon the most appropriate thermal cycle. Peak temperature and time were selected to develop ASTM grain size in the range of 4 to 5. The peak temperature was limited to 1260°C (2300°F), specifically to be below the burning temperature for steels of typical RPV chemistry [1]. The thermal cycle used is shown in Fig. 4. Specimen blanks prepared for the Gleeble were cylindrical rods about 76 mm long and 14.35 mm in diameter (3 by 0.564 in.). About 5 mm (0.2 in.) of material at the center of each rod was determined to be representative of the weld cycle material. An example photomicrograph of the resulting microstructure appears in Fig. 5, showing a mixture of martensite and lower bainite.

Table 7 lists the Gleeble weld-simulation and aging data developed to date. The PWHT cycle was identical to that used in the AEA-Technology simulation (namely, a 24-h soak time at 615°C (1140°F) followed by an oil quench). The as-tempered toughness reflects a favorable microstructural condition that in all probability resulted from the fast cooling of the weld-cycle simulation. Aging time at 168 h represents the expected hold time that would be used in an RPV annealing procedure. Three aging temperatures represent the lowest to highest practical annealing temperatures that have been under consideration [399, 450, and 482°C (750, 842, and 900°F)]. At 399°C, there appears to be no evidence of temper embrittlement in four materials. This arguably could also be true for the high-phosphorus modified A 302 grade B steel (Z5) that for a lack of sufficient material was not included in this aging exposure. However, at 450 and 482°C,

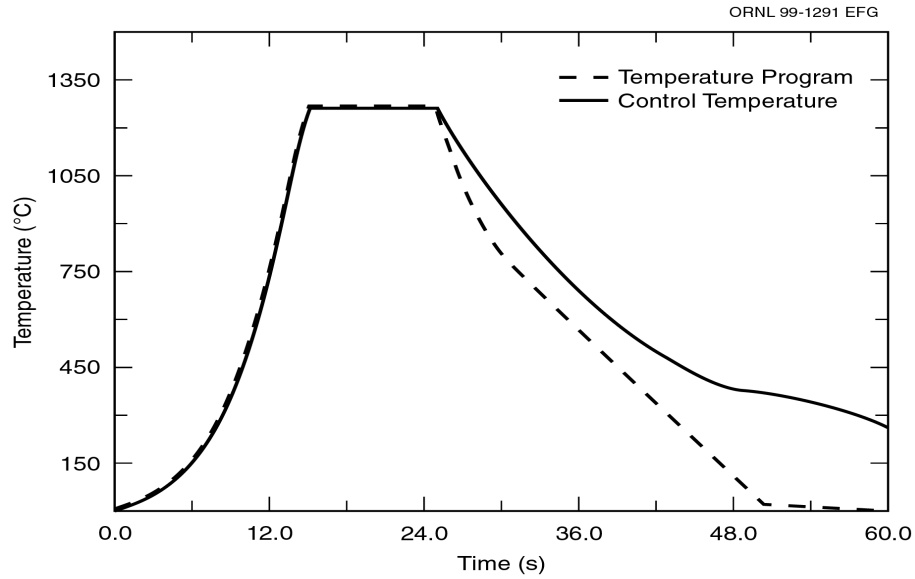


Figure 4. Gleeble-generated weld thermal cycle to develop ASTM 4.5 grain size.



98-1734-01 MOD A302 B #2 356 -100C 100X 50µm

Figure 5. Photomicrograph of the microstructure of the high-phosphorus modified A302 grade B steel after Gleeble austenitize and postweld heat treatment, nital etch, 100 \times .

Table 7. Charpy Impact Transition Temperatures for ORNL Materials Austenitized by Gleeble, PWHT, and Thermal Aging

| Austenitize method | Aging temperature (°C) | Aging time (h) | Transition temperature, T_0 , and change in T_0 (ΔT_0) (°C) | | | | |
|--------------------|------------------------|----------------|---|--------------|--------------|-------------------------|--------------|
| | | | A302B | A533B | A508 class 2 | Modified A302B | |
| | | | | | | High P | Low P |
| Gleeble | Initial | 0 | -87 | -67.0 | -102 | — (—) | -67 |
| Gleeble | 399 | 168 | — (—) | -67.1 (-0.1) | -98.6 (3.4) | -89.4 (0) ^a | -71.1(-4.1) |
| Gleeble | 450 | 168 | -44 (43) | -28 (39) | -80 (22) | — (—) | -47 (20) |
| Gleeble | 482 | 168 | — (—) | 7.4 (74.4) | -72.6 (29.4) | -47.4 (42) ^a | -33.6 (33.4) |
| Gleeble | 450 | 2000 | 43 (130) | 66 (133) | -46 (56) | 14 (75.4) ^a | -4 (63) |

^aEstimated change assuming initial T_0 is the same as that following aging at 399°C for 168 h.

embrittlement develops and increases with increasing temperature. Hence, these two annealing conditions produce temper embrittlement damage, provided there is coarse grain HAZ material. However, Fig. 6 shows that, after the samples were annealed for 168 h, none of the transition temperatures exceeded room temperature. After 2000 h at 450°C, two of the five materials had T_0 temperatures that exceeded room temperature, with ΔT_0 values of 130 and 133°C. Scanning electron fractography was performed on the modified low-phosphorus A302B steel in the Gleeble/PWHT condition after aging at 450°C for 168 h and 2000 h, and for the high-phosphorus steel after 2000-h aging only. After 168 h of aging, the Charpy impact fracture surface of the low-phosphorus steel exhibited mixed cleavage and intergranular fracture. In this case, intergranular fracture was the predominant mode in the region near the notch tip, but cleavage fracture was the predominant mode for the bulk of the fracture surface away from the near-notch region. However, in the case of the material aged for 2000 h, the fracture surface exhibited predominantly intergranular fracture throughout, and this observation applied to both the low- and high-phosphorus steels. At higher test temperatures, where the Charpy energy was on the upper shelf, fractography showed only ductile void coalescence for both the low- and high-phosphorus steels after 2000 h.

Six commercial welds were examined for maximum grain size along the fusion line (Table 8). The results of this small sampling of actual RPV welds suggested that the presumed coarse grain size and uniform distribution characteristics do not always exist. The coarse grains that were identified were much smaller than ASTM 4.5, and the percentage of coarse grains along all fusion lines was found to be very low. Example photomicrographs taken at selected large-grain locations are provided in Ref. 1.

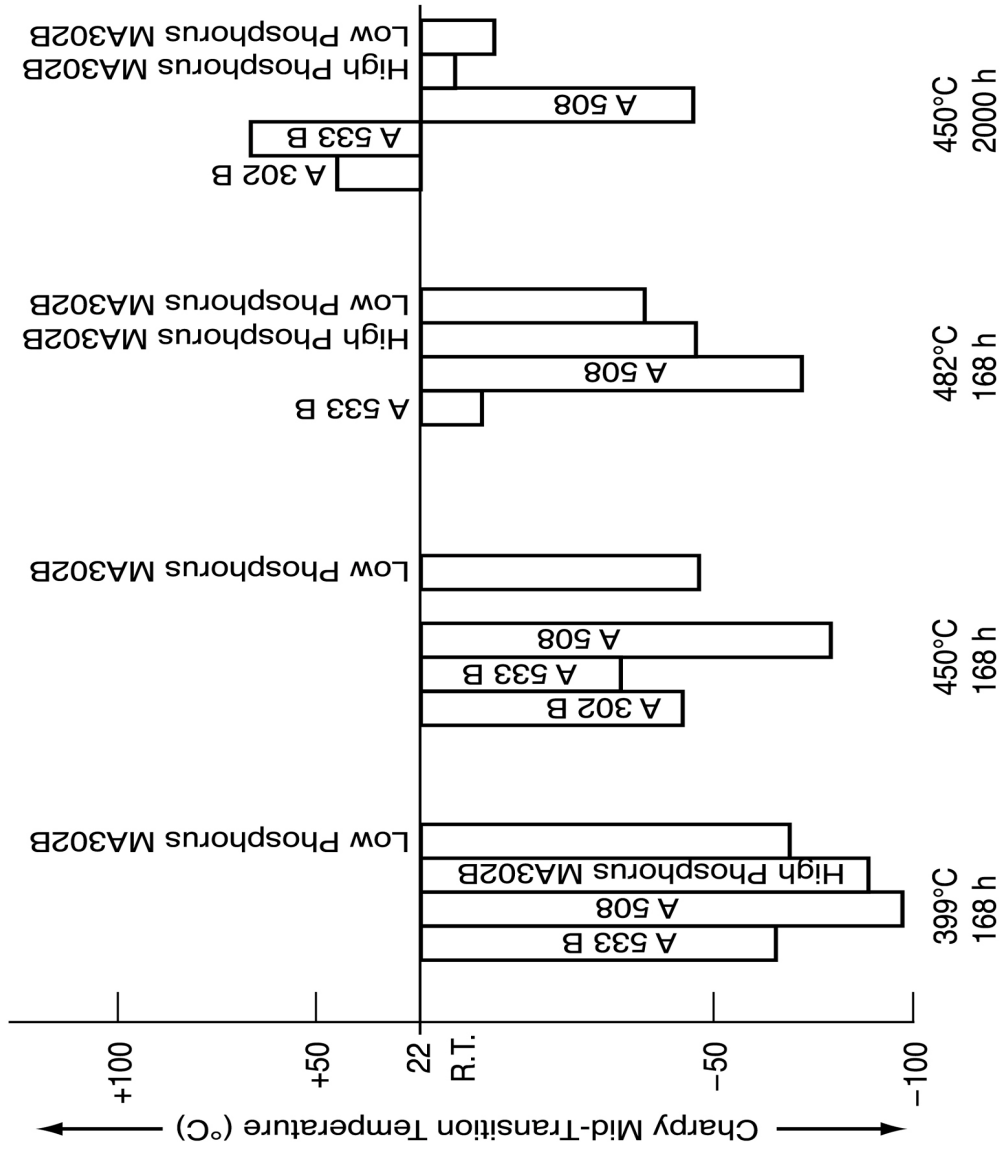


Figure 6. Charpy impact mid-transition temperatures after aging for 168 h at 399, 450, and 482°C (750, 842, and 900 °F) and 2000 h at 450°C (MA302B).

Table 8. Largest Coarse Grain Sizes Found in HAZs of Six Commercially Fabricated RPV Welds

| Weld source | ASTM E 112 grain size |
|------------------------------------|-----------------------|
| HSSI Fifth Irradiation Series, 72W | 6.5 |
| HSSI Fifth Irradiation Series, 73W | 9.0 |
| SNUPPS beltline | 7.5 |
| SNUPPS longitudinal | 7.5 |
| Midland beltline | 10 |
| Midland nozzle course | 6.5 |

Measurement of Element Diffusion to Grain Boundaries

Measurement of element diffusion to grain boundaries was conducted as part of a collaboration with AEA-Technology, Harwell, United Kingdom. The segregation of critical elements to grain boundaries on four selected specimens was measured by scanning transmission electron microscopy/energy dispersive X-ray analysis (STEM/EDX). These results were then compared with theoretical calculations by using the McClean model [10] as well as the Murphy and Perks model [11]. Experimental results are shown in Table 9. The grain-boundary analyses also included Cu, Si, and Cr; low levels of segregation were observed. Measurement replication was four times, and in some cases the variability was very large. Phosphorus segregation to grain boundaries was also calculated. The McClean equation reasonably predicted segregated concentrations of all the modified A302B specimens but not for the A533B specimens; the likely reason is that the bulk phosphorus given in Table 2 was used in the calculation instead of the more recent phosphorus determinations that appear in Table 3.

Table 9. AEA-Technology Measurements of Grain Boundary Phosphorus Coverage

| Material | Treatments | Equivalent monolayer coverage (%) | | | |
|------------------------------------|--|-----------------------------------|----|----|-----|
| | | Mn | Mo | P | Ni |
| Modified A 302 B (low phosphorus) | Gleeble austenitized and PWHT (unaged) | 9 | 12 | 1 | 1 |
| Modified A 302 B (low phosphorus) | Gleeble austenitized and PWHT (aged at 450 °C, 2000 h) | 19 | 16 | 10 | 1.5 |
| Modified A 302 B (high phosphorus) | Gleeble austenitized and PWHT (aged at 450 °C, 2000 h) | 14 | 32 | 17 | 8 |
| A 533 grade B (high phosphorus) | Gleeble austenitized and PWHT (aged at 450 °C, 2000 h) | 19 | 15 | 5 | 10 |

One sample analyzed by AEA [A 533 grade B steel that had been Gleeble-austenitized and aged at 450°C (842°F)] also underwent Auger analysis at ORNL. (In this method, a fresh fracture surface is created under vacuum and analyzed.) Part of the surface was intergranular, exposing the grain boundaries (GBs), as shown in Fig. 7; the other part of the surface had transgranular (TG) cleavage. Bulk phosphorus was determined on TG cleavage surfaces and on GBs after a thickness of 10 Å was removed by sputtering (SP) (see Fig. 7). On average, the difference between bulk and GB phosphorus is a factor of about 10. A number of other elements were also measured; Table 10 summarizes the observations in terms of the change from the levels measured within the grains. As observed in the AEA-Technology STEM/EDX measurements, molybdenum is a significant segregant, primarily because it is strongly attracted to phosphorus. As further shown in Ref. 1, intergranular fracture vanishes at Charpy upper-shelf test temperatures.

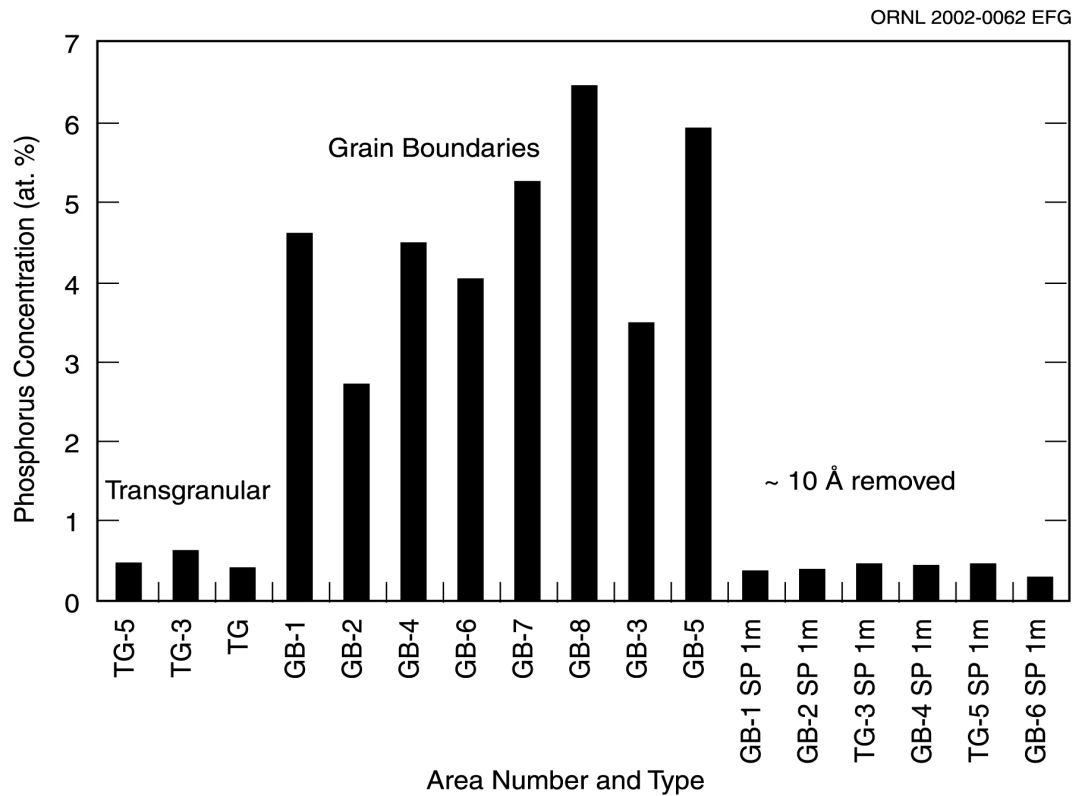


Figure 7. Auger analysis of phosphorus concentration in A533 grade B class 1 following Gleeble austenitization and thermal aging at 450°C (842°F) for 2000 h. (TG: Transgranular; GB: grain boundary; SP: sputtered)

Table 10. Results of Auger Analysis on A533 Steel in the Gleeble/PWHT Condition Aged at 450°C (842°F) for 2000 h

| | Composition (at. %) | | | | | | |
|--------------------------|------------------------|------|------|------|------|------|------|
| | P | Mo | C | O | Fe | Ni | Cu |
| Average intergranular | 0.50 | x | x | x | x | x | x |
| Average grain boundaries | 4.62 | 6.3x | 2.0x | 0.9x | 0.8x | 1.8x | 2.6x |

Effects of Irradiation and Thermal Annealing

The low-phosphorus modified A302B steel was selected for the first irradiation and annealing experiment. A total of 30 Charpy impact specimens (3 groups of 10 specimens each) was machined, one group from the as-received plate and two groups from the Gleeble-austenitized/PWHT material. The specimens were irradiated in the HSSI Irradiation, Annealing, and Reirradiation (IAR) facility at the University of Michigan Ford Reactor at an irradiation temperature of 288°C ± 2°C (550°F ± 4°F). The specimens were exposed to a fluence of about 1 × 10¹⁹ n/cm² (1 MeV) at a flux of about 4 × 10¹¹ n/cm²/s. One group of the Gleeble treated specimens was subsequently annealed at 460°C ± 2°C (860°F ± 4°F) for 168 h in air in a hot cell at ORNL. The specimens were then tested at various temperatures, and scanning electron fractography was performed on selected specimens from each group. Table 11 provides a summary of the CVN results for the three groups and, for comparison, for the Gleeble/PWHT material after thermal aging only. The material is not very radiation sensitive, as shown by the relatively low transition temperature shift of 22°C. The unirradiated material was also aged at the irradiation temperature of 288°C for approximately the same time as the irradiation exposure (119 days); as the results show, there was no effect of such low-temperature aging. The expected effect of postirradiation thermal annealing at 460°C for 168 h would be nearly full recovery of the transition temperature. In this case, however, the transition temperature did not recover, perhaps indicative of another operative metallurgical mechanism in the material. Although hardness or tensile tests have not yet been performed, the USE increase after annealing to a level greater than that of the unirradiated condition is similar to other observations, at least implying that radiation hardening may have decreased as a consequence of the annealing treatment. Similarly, the material aged at 450°C (842°F) for 168 h shows the same effect. This finding further supports the possibility of another mechanism of embrittlement.

Table 11. Summary of Irradiation, Annealing, and Thermal Aging Effects on Simulated HAZ in A302B (Modified) Steel

| Condition | Charpy impact mid-transition (°C) | | Charpy upper-shelf energy (J) | |
|-----------------------|-----------------------------------|-----------------|-------------------------------|------|
| | T _o | ΔT _o | USE | ΔUSE |
| Gleeble initial | -67 | – | 129 | – |
| Irradiated | -45 | 22 | 121 | -8 |
| Irradiated/Annealed | -38 | 29 | 140 | 11 |
| Aged 288°C/119 days | -70 | -3 | 117 | -12 |
| Aged 450°C/168 hours | -47 | 20 | 141 | 12 |
| Aged 450°C/2000 hours | -4 | 63 | 129 | 0 |

Scanning electron fractography was performed on an XL-30 Philips scanning electron microscope in an ORNL hot cell. Figure 8 shows that cleavage was the dominant fracture mechanism in the as-received plate after irradiation; no intergranular fracture was observed. Figure 9 shows the Gleeble/PWHT material after irradiation; cleavage fracture is the dominant mechanism; in this case, however, about 15% intergranular fracture was observed. Figures 10 and 11 show fractographs for two different specimens of the Gleeble/PWHT steel in the irradiated/annealed condition. Both specimens exhibit significant intergranular fracture, with the fraction of intergranular fracture appearing somewhat greater in the specimen that failed at higher energy. Figures 12(a) and (b) show higher-magnification fractographs of the specimen in Fig. 11. It is apparent that intergranular fracture is the predominant mechanism of failure of this material, with the fraction of intergranular fracture being greater than 75% of the fracture surface.

DISCUSSION

Experiments at AEA-Technology have clearly demonstrated that steels with the typical RPV chemistry can be made to be highly sensitive to temper embrittlement if the prior-austenite grain size is enlarged to more than 360 μm in diameter. The SAW process used in RPV fabrication is a high-heat-input welding procedure, and grains of substantial enlargement would seem quite likely, more so than in offshore shielded-metal arc weldments. Hence, there was a need to pursue more information on temper embrittlement. The scope of interest comprised the temper-embrittlement properties of commercially made RPV steels, the influence of grain-size and thermal-cycle effects, and the effects of neutron irradiation and thermal annealing.

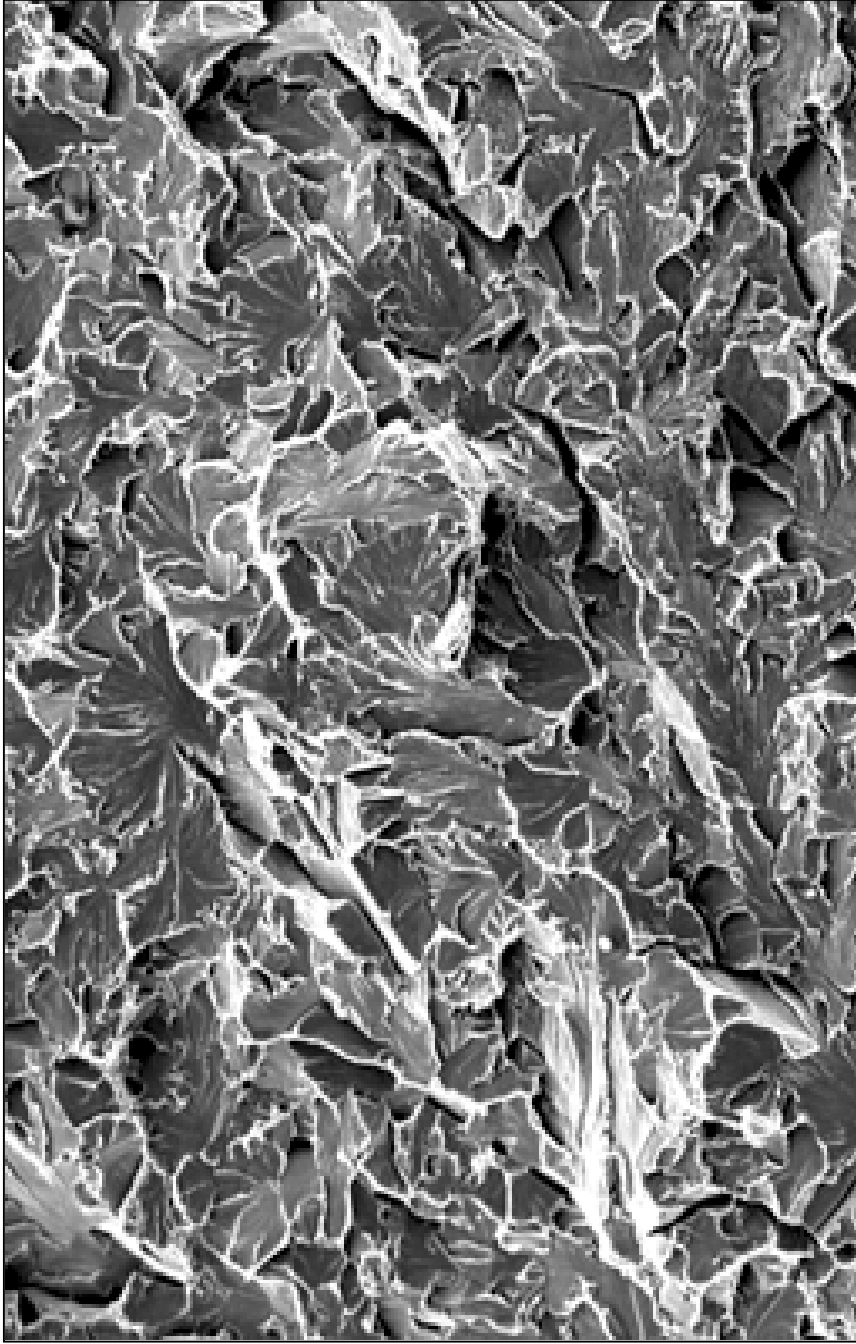


Figure 8. Scanning electron fractograph of as-received modified A302B steel Charpy impact specimen following irradiation at 288 °C (550 °F) to 1×10^{19} n/cm².

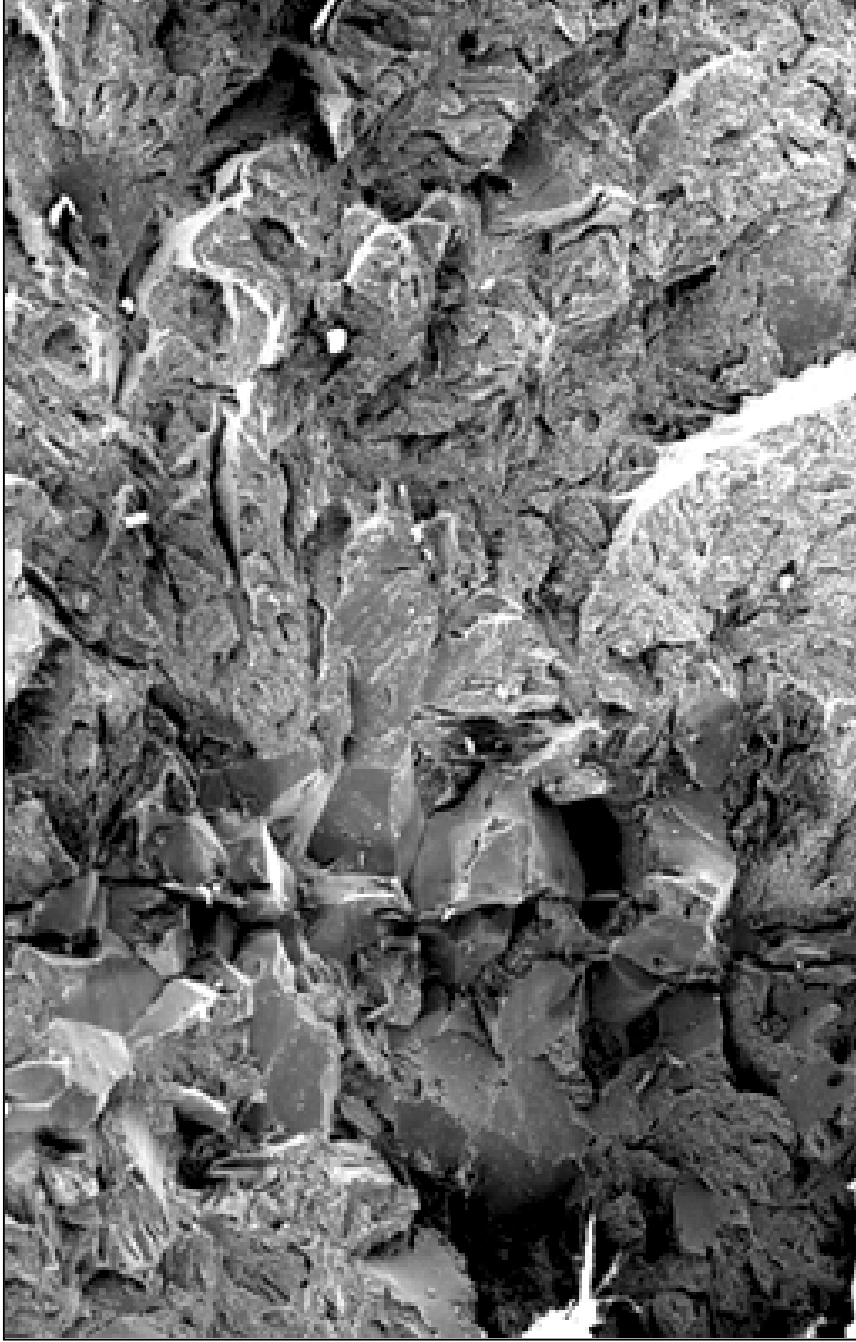


Figure 9. Scanning electron fractograph of Gleeble austenitized/PWHT modified A302B steel Charpy impact specimen following irradiation at 288 °C (550 °F) to 1×10^{19} n/cm².

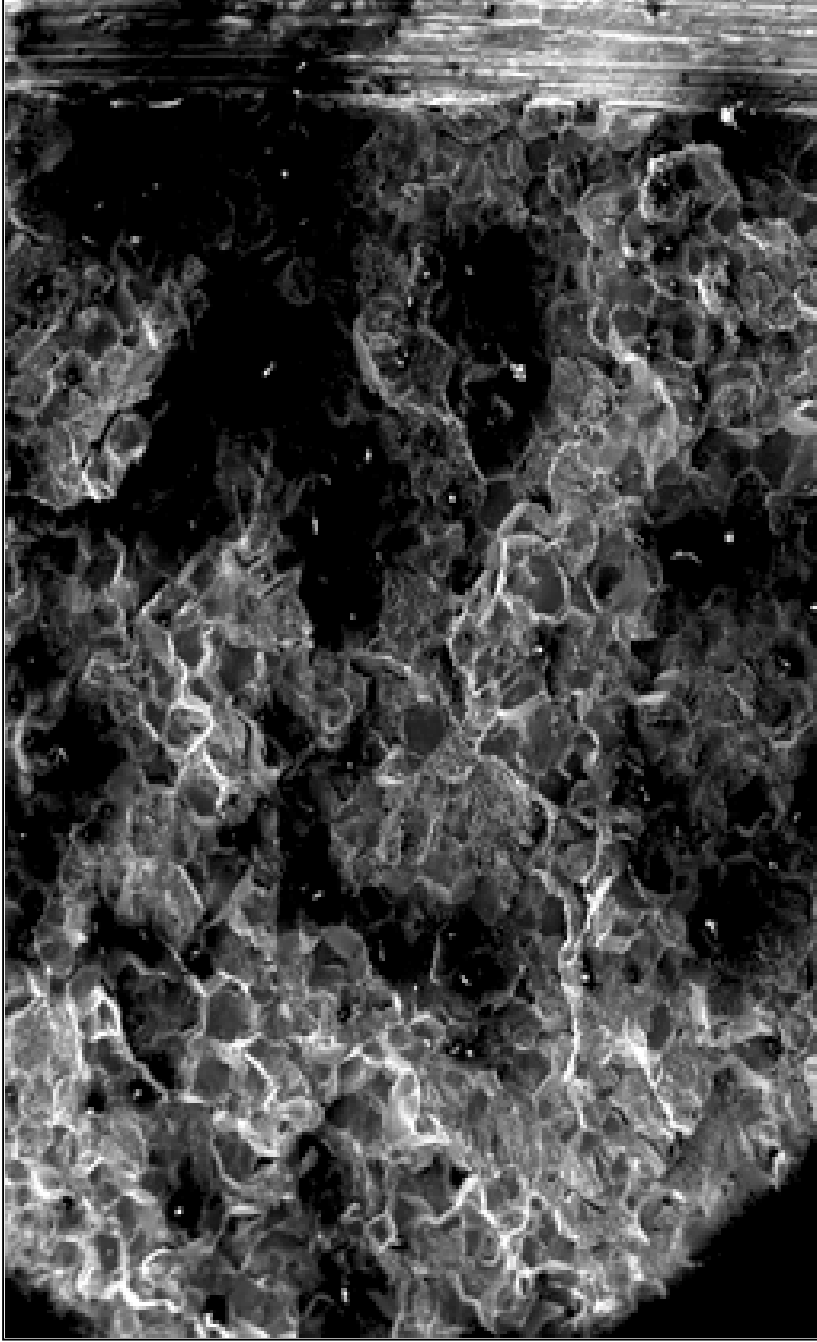


Figure 10. Scanning electron fractograph of Gleeble austenitized/PWHT modified A302B steel Charpy impact specimen following irradiation at 288°C (550°F) to 1×10^{19} n/cm² and thermal annealing at 460°C (860°F) for 168 h. Specimen failed with 4 J. The notch of the specimen appears at the right side of the fractograph.

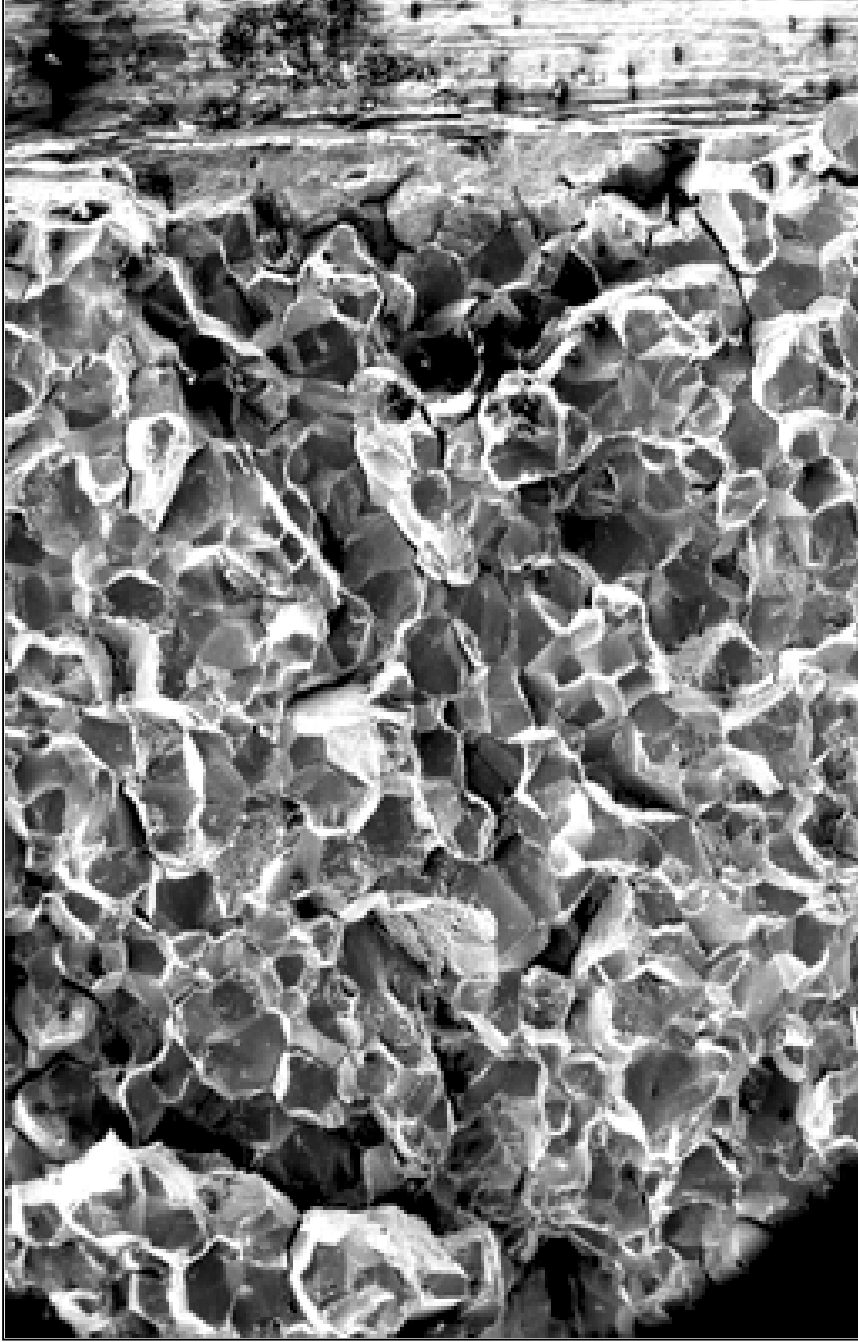


Figure 11. Scanning electron fractograph of Gleeble austenitized/PWHT modified A302B steel Charpy impact specimen following irradiation at 288 °C (550 °F) to 1×10^{19} n/cm² and thermal annealing at 460 °C (860 °F) for 168 h. Specimen failed with about 37 J. The notch of the specimen appears at the right side of the fractograph.

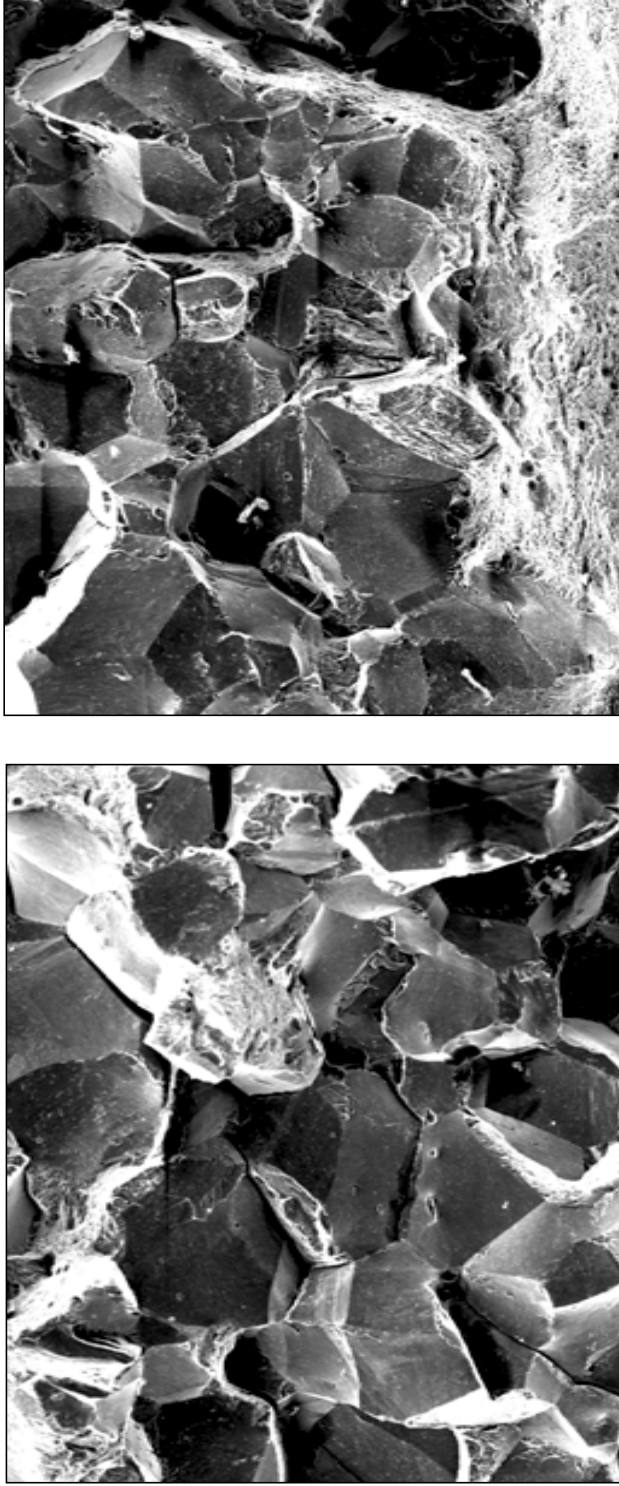


Figure 12. Scanning electron fractographs of Gleeble austenitized/PWHT modified A302B steel Charpy impact specimen following irradiation at 288 °C (550 °F) to 1×10^{19} n/cm² and thermal annealing at 460 °C (860 °F) for 168 h showing (a) region near crack front and (b) region near one side of the specimen showing shear lip area. (Higher magnification of same specimen is shown in Fig. 11.)

The objective of Phase I was to confirm the AEA-Technology findings, except in this case commercially made steels were used. This work clearly showed that the temper embrittlement seen with the AEA-Technology laboratory-made steels did in fact apply to the five selected commercially made steels. However, the CVN ΔT_0 magnitude was somewhat less.

Phase II introduced an anticipated more-representative weld HAZ coarse grain size as well as the heating and cooling rates of a typical weld pass. Most RPV steels have CE of about twice that of microalloyed steels. Consequently, the transformation products formed with the high cooling rates of a weld pass are favorable for the development of high fracture toughness if postweld stress-relief tempering is used. All of the commercial steels had exceptionally good (low-temperature) preaged transition temperatures after simulated weld cycles. Given a 168-h anneal at 450°C (842°F), the fracture toughness was degraded, but not as much as the fracture toughness improved from the austenitization and PWHT cycle. The rapid cooling after PWHT should maximize the temper embrittlement sensitivity.

Phase III expanded the study to look at other aging-condition variables. The austenitization, PWHT, and grain size were the same as in Phase II. Aging time was fixed at 168 h, but aging temperature was varied. Given the aging times used, a lower-bound aging temperature for temper embrittlement was observed. At 399°C (750°F) there was no detectable temper embrittlement in any of the steels. At 450 and 482°C (842 and 900°F), significant transition-temperature shifts could be seen. However, there were no postembrittlement T_0 temperatures observed above room temperature as the result of aging for 168 h.

Irradiation experiments were performed to determine whether an RPV steel with demonstrated temper-embrittlement insensitivity at temperatures below 400°C (752°F) can suffer embrittlement at 288°C (550°F) when the thermal exposure is combined with neutron irradiation or when irradiation is followed by postirradiation annealing at about 454°C (849°F) for 168 h, a process intended to recover fracture toughness. The results for one relatively low-phosphorus RPV steel, initially heat-treated to simulate the coarse grain microstructure in an RPV submerged-arc weldment, have indicated a surprising propensity for temper embrittlement following irradiation and thermal annealing. Calculations of irradiation-induced segregation of phosphorus using the Murphy-Perks model were made by AEA-Technology. It was concluded that irradiation appears to have a similar effect to a 482°C (900°F), 168-h thermal aging treatment if the initial segregation level is allowed to be representative of the PWHT condition. Although the results indicate that the monolayer coverage could be on the order of 10%, the postirradiation annealing treatment would not be expected to deposit sufficient additional phosphorus to result in such a high fraction of intergranular fracture. Additional such calculations will be performed, but measurements of elemental segregation to the grain boundaries in that steel are highly desirable to confirm the nature of the segregation. The role of molybdenum in this case is implicated, as is the potential role of free carbon.

SUMMARY OF OBSERVATIONS AND CONCLUSIONS

Local grain-coarsened regions in simulated RPV weld HAZs of five representative RPV materials have been studied. Two grain-coarsening schedules have been used: (1) the AEA-Technology cycle for prior austenite grain growth creates massive grains to determine whether the extremely large Charpy ΔT_0 values observed in the AEA-Technology model alloys are representative of commercial RPV alloys, and (2) the Gleeble cycle for prior austenite grain growth creates coarse grain sizes representative of multipass weld LBZs. The thermal history is prototypic of SAW cycles, except that rapid cooling was imposed following the PWHT.

1. No examples of structural failures traced to LBZ in RPV welds were found in the literature.
2. Thermal aging at 450°C (842°F) for 2000 h of Gleeble-simulated HAZs resulted in almost complete intergranular fracture of A533B (P = 0.18%) and modified A302B (P = 0.007%) steels and a factor of 10 higher grain boundary phosphorus content in A533B.
3. The McClean model of phosphorus segregation reasonably predicted the measured results.
4. Irradiation of a Gleeble-simulated HAZ in modified A302B steel (P = 0.007%) to 1.0×10^{19} n/cm² (>1 MeV) at 288°C (550°F) showed the following:
 - a. The irradiation-induced Charpy shift was 22°C.
 - b. Thermal annealing at 450°C for 168 h produced no recovery of transition toughness.
 - c. Irradiated specimens exhibited about 10 to 20% intergranular fracture.
 - d. After thermal annealing at 460°C (860°F) for 168 h, specimens exhibited more than 75% intergranular fracture.
5. Microscopic examination is required to explain the causes of such extensive intergranular fracture in this particular low-phosphorus steel. Further experiments with the same steel given a prototypic cooling rate following the PWHT are recommended.

ACKNOWLEDGMENTS

This research was sponsored by the Office of Nuclear Regulatory Research, U.S. Nuclear Regulatory Commission, under Interagency Agreement DOE 1886-N695-3W with the U.S. Department of Energy under Contract No. DE-AC05-00OR22725 with UT-Battelle, LLC. The authors are indebted to the late Michael Vassilaros of the NRC who assisted with the evaluations of this work during the aging studies. Assistance at ORNL of the following individuals is also greatly appreciated: Lee Heatherly for Auger analysis, Alan Frederick for Gleeble austenitization, Edward Hatfield for heat treatment, Janie Gardner and Jackie Mayotte for metallography, Ronald Swain and Eric Manneschmidt for mechanical tests, James King for welding technology guidance, and Julia Bishop for preparation of the manuscript.

REFERENCES

- [1] McCabe, D. E., *Initial Evaluation of the Heat-Affected Zone, Local Embrittlement Phenomenon as it Applies to Nuclear Reactor Vessels*, ORNL/NRC/LTR-99/10, September 1999.
- [2] Barnes, A. M., *The Effect of Intercritical Thermal Cycles on HAZ Microstructure and Toughness in C-Mn-Al-Nb Steel*, Report 402/1989, The Welding Institute, August 1989.
- [3] Arimochi, K., "CTOD Behavior of Steel Weld with 500 MPa Class Strength and HAZ-CTOD Characteristics of Newly Developed Low Al-B-N Steel," *Transactions of the Japan Welding Society*, 20(2), 1989.
- [4] Thaulow, C., and Paaw, A. J., "Materials Characterization with Respect to HAZ Local Brittle Zones," *WELDTECH* 88, London, November 1988, pp. 24-1 to 24-14.
- [5] McElroy, R. J., Foreman, A. J. E., Gage, G., Phythian, W. J., Ray, P. H. N., and Vatter, I. A., "Optimization of Reactor Pressure Vessel Surveillance Programmes and Their Analysis," contribution to IAEA CRP 3 Research Program, AEA-RS-2426, December 1993.
- [6] J. A. Wang, *Embrittlement Data Base, Version 1*, USNRC Report NUREG/CR-5506 (ORNL/TM-13327), August 1999.
- [7] Nanstad, R. K., McCabe, D. E., Swain, R. L., and Miller, M. K., *Chemical Composition and RT_{NDT} Determination for Midland Weld WF-70*, NUREG/CR-5914 (ORNL-6740), 1992.
- [8] Nanstad, R. K., McCabe, D. E., and Swain, R. L., "Evaluation of Variability in Material Properties and Chemical Composition for Midland Reactor Weld WF-70," *Effects of Radiation on Materials: 18th International Symposium, ASTM STP 1325*, R. K. Nanstad, M. L. Hamilton, F. A. Garner, and A. S. Kumar, Eds., American Society for Testing and Materials, West Conshohocken, PA, 1999, pp. 125–56.
- [9] C. D. Lundin and S. Mohammed, *Effect of Welding Conditions on Transformation and Properties of Heat-Affected Zones in LWR Vessel Steels*, USNRC Report NUREG/CR-3873 (ORNL/SUB/78-7637/1), November 1990.
- [10] McClean, D., *Grain Boundaries in Metals*, Clarendon Press, Oxford (1957).
- [11] Druce, S. G., Gage, G., and Jordan, G. R., *Acta Metallurgica*, 34, 1986, pp. 641–52.

DISTRIBUTION

INTERNAL

- | | | | |
|-----|-----------------|--------|--|
| 1. | B. R. Bass | 12. | G. E. Michaels |
| 2. | E. E. Bloom | 13. | M. K. Miller |
| 3. | T. S. Byun | 14. | D. L. Moses |
| 4. | W. R. Corwin | 15-19. | R. K. Nanstad |
| 5. | S. A. David | 20. | J. B. Roberto |
| 6. | K. Farrell | 21-28. | T. M. Rosseel |
| 7. | R. G. Gilliland | 29. | J. J. Simpson |
| 8. | L. L. Horton | 30. | L. L. Snead |
| 9. | R. L. Klueh | 31-33. | M. A. Sokolov |
| 10. | L. K. Mansur | 34. | R. E. Stoller |
| 11. | J. G. Merkle | 35. | S. J. Zinkle |
| | | 36. | Office of Technical Information and Classification |
| | | 37. | Central Research Library |

EXTERNAL

38. N. C. Chokshi, RES/DET/MEB, U.S. Nuclear Regulatory Commission, Washington, DC 20555-0001
39. M. E. Mayfield, RES/DET/MEB, U.S. Nuclear Regulatory Commission, Washington, DC 20555-0001
40. E. M. Hackett, RES/DET/MEB, U.S. Nuclear Regulatory Commission, Washington, DC 20555-0001
41. M. T. Kirk, RES/DET/MEB, U.S. Nuclear Regulatory Commission, Washington, DC 20555-0001
42. C. J. Fairbanks, RES/DET/MEB, U.S. Nuclear Regulatory Commission, Washington, DC 20555-0001
43. S.N.M. Malik, RES/DET/MEB, U.S. Nuclear Regulatory Commission, Washington, DC 20555-0001
44. C. G. Santos, NMSS/SFPO, U.S. Nuclear Regulatory Commission, Washington, DC 20555-0001
- 45-47. C. A. English, AEA-Technology, Harwell Laboratory, Didcot, Oxfordshire, OX11 0RA, United Kingdom
48. R. L. Faulkner, Loughborough University of Technology, Loughborough, Leics LE11 3TU, United Kingdom

49. T. Griesbach, ATI Consulting, 2010 Crow Canyon Place, Suite 140, San Ramon, CA 94583
50. R. Lott, Westinghouse, 1310 Beulah Rd., Pittsburgh, PA 15325
51. G. E. Lucas, Department of Mechanical Engineering, University of California, Ward Memorial Drive, Santa Barbara, CA 93106
- 52-54. D. E. McCabe, 124 Newport Drive, Oak Ridge, TN 37830
55. G. R. Odette, Department of Mechanical Engineering, University of California, Ward Memorial Drive, Santa Barbara, CA 93106
- 56-58. S. R. Ortner, AEA-Technology, Harwell Laboratory, Didcot, Oxfordshire, OX11 0RA, United Kingdom
59. S. T. Rosinski, EPRI, 1300 W. Wt. Harris Blvd., Charlotte, NC 28262-8550
60. W. L. Server, ATI Consulting, 24 Grenbarr Ct., Pinehurst, NC 28374